

Article

Effect of Surface Nanocrystallization on Corrosion Resistance of the Conformed Cu-0.4%Mg Alloy in NaCl Solution

Dan Song^{1,2}, Jinghua Jiang^{1,*}, Xiaonan Guan¹, Yanxin Qiao³ , Xuebin Li⁴, Jianqing Chen¹, Jiapeng Sun¹  and Aibin Ma^{1,2,*}

¹ College of Mechanics and Materials, Hohai University, Nanjing 210098, China; songdancharls@hhu.edu.cn (D.S.); guanxiaonanayln123@163.com (X.G.); chenjq@hhu.edu.cn (J.C.); sun.jiap@gmail.com (J.S.)

² Suqian Research Institute, Hohai University, Suqian 223800, China

³ School of Materials Science and Engineering, Jiansgu University of Science and Technology, Zhenjiang 212003, China; yxqiao@just.edu.cn

⁴ China Railway Construction Electrification Bureau Group Co., Ltd., Beijing 100043, China; xblee2013@sohu.com

* Correspondence: jinghua-jiang@hhu.edu.cn (J.J.); aibin-ma@hhu.edu.cn (A.M.); Tel.: +86-25-8378-7239 (J.J. & A.M.); Fax: +86-25-8378-6046 (J.J. & A.M.)

Received: 28 August 2018; Accepted: 25 September 2018; Published: 26 September 2018



Abstract: Surface nano-crystallization (SNC) of a conform-extruded Cu-0.4 wt.% Mg alloy was successfully conducted by high-speed rotating wire-brushing to obtain the deformed zone with dislocation cells and nanocrystallines. SNC promotes the anodic dissolution and corrosion rate of the Cu-Mg alloy in the initial stage of immersion corrosion in 0.1 M NaCl solution. The weakened corrosion resistance is mainly attributed to the higher corrosion activity of SNC-treated alloy. With extending the immersion time, the SNC-treated alloy slows the corrosion rate dramatically and exhibits uniform dissolution of the surface. The formation of the dense corrosion products leads to the improvement of overall corrosion performance. It indicates that the SNC-treated Cu-Mg alloy can function reliably for a longer duration in a corrosive environment.

Keywords: Cu-Mg alloy; conform; surface nanocrystallization; corrosion resistance

1. Introduction

With the rapid growth of the high-speed railway over the last few decades, more attention has been focused on the development of copper alloys for their high strength, good electrical conductivity, satisfactory resistance to wear, and corrosion for contact wires [1]. Until now, plenty of research has been conducted to enhance the required properties of copper alloys by adding small amounts of alloying elements to them, such as Cr, Zr, Ag, Ni, and Mg [2–6]. Contact wire Cu-Mg alloys with lower production costs demonstrate ideal comprehensive properties and are considered the current preferred material for making contact wires for high-speed trains, of which the operating speed is more than 300 km/h [7,8]. According to the phase diagram of Cu-Mg, a single solid-solution copper alloy containing a small amount of Mg can be obtained at room temperature. Solution strengthening of the Mg element should not cause severe lattice distortion of the copper matrix for their similar atom radius, and should therefore keep the excellent conductivity performance of copper. In China, Cu-Mg contact wires are now widely used in trains running at the speed of ≥ 300 km [7]. Compared with other copper alloys, single solid-solution Cu-Mg alloys have good comprehensive performance, a simple manufacturing process, and vast application prospects. In their long-term operation, they can

hardly be immune from water, humidity, and salts, which affect the lifespan of contact wires. By all appearances, the corrosion control of Cu-Mg alloys is a valuable research issue.

According to the Hall Petch equation, fine grains can improve the strength of materials, and as it is generally believed, grain refinement can simultaneously benefit strength and toughness. Grain refinement of single solid-solution Cu-Mg alloy have been applied to achieve a good combination of strength and conductivity. At present, the China Railway Construction Electrification Bureau Group (Kang Yuan New Materials Co., Ltd.) has developed fine-grained Cu-0.4 wt.% Mg contact wire by using the conform-process, as well as cold drawing. The severe plastic deformation (SPD) procedure is currently one of the most effective ways to produce ultrafine-grained (UFG) alloys, which is gaining an increasing amount of attention [9–11].

Surface nano-crystallization (SNC) can be used to induce severe plastic deformation in the surface layer and obtain a nano-cystallized/ultrafine-grained (NC/UFG) gradient layer with high strength and hardness [12,13]. The enhanced mechanical properties, especially the enhanced surface hardness, will improve the wear resistance of the contact wire and decrease its wear loss induced by the sliding friction with the pantograph. However, due to the complex electrochemical corrosion process and various influencing factors, it still cannot get a unified conclusion to the effect of SNC on the corrosion behavior of treated metals. Some studies reported that the SNC process decreased the corrosion resistance of the metals. Li [14] declared the decreased corrosion resistance of SNC low-carbon steel due to the increased number of active corrosion sites. Others reported the positive effect of SNC on the anti-corrosion performance of the treated metals, such as improved corrosion resistance of the SNC 316L SS steel [15] and AISI 409 SS steel [13] by surface mechanical attrition treatment (SMAT). Our former investigation also found improved passivation ability and corrosion resistance of the SNC-treated low-carbon steel rebar in the Cl^- -containing concrete pore solution [16].

As important as it is to develop high-strength, good-conductivity copper contact wires, the present work investigates the corrosion behavior and corrosion resistance of the on-line conformed Cu-0.4wt.% Mg alloy subjected to experimental SNC processes by high-speed wire-brushing [16]. The influential mechanism of the SNC process on the corrosion behavior of this alloy was systematically studied. The SNC-induced special surface microstructure and surface roughness have a close relationship to the evolution in unique corrosion behavior of this alloy.

2. Experiment

The material used was Cu-0.4 wt.% Mg (oxygen \leq 10 ppm) alloy, which were melted with electrolytic copper and pure magnesium through upward-casting, and then extruded by the conform process of the China Railway Construction Electrification Bureau Group (Kang Yuan New Materials Co., Ltd., Jiangsu, China). Mg atoms of the binary alloy mainly existed at the FCC-structured copper crystal. An illustration of the conform process is presented in Figure 1, which clearly shows it is able to refine the grain size of the alloy, and thus simultaneously improve its strength, plasticity, and conductivity [17]. The conformed round bars were continuously treated by SNC-processing via a high-speed rotating wire brush, which inflicts severe plastic deformation to the sample surface by forceful and repeated scratching (as shown in Figure 2). The detailed SNC processing parameter, such as rotation speed of the wire brush and the feeding speed of the sample, can be found in our former work [16]. Each sample was SNC-processed for four passes to obtain a uniformly modified surface layer and extreme grain refinement on the brushed surface. An optical microscope (Olympus BX51M, Tokyo, Japan) was used to observe the microstructure at the surface of the brushed samples. The composition of the etchant was glacial acetic acid 5 mL, phosphoric acid 11 mL, and nitric acid 4 mL. The etching time was 5 s. Transmission electron microscopy (TEM, JEM-2000EX, Tokyo, Japan) was applied to observe the microstructure and grain size of the Cu-Mg alloy after SNC processing. X-ray diffraction (XRD) analysis of the samples was performed using a Bruker D8 Advance diffractometer (Bruker AXS, Karlsruhe, Germany) with Cu K 1 radiation. The θ - 2θ diffraction patterns were scanned from 15° to 85° with a scanning rate of 2° min^{-1} . The laser scanning confocal microscope (Olympus

LEXT OLS4000 3D, Tokyo, Japan) was used to quantitatively analysis the surface roughness after SNC treatment of the alloy.

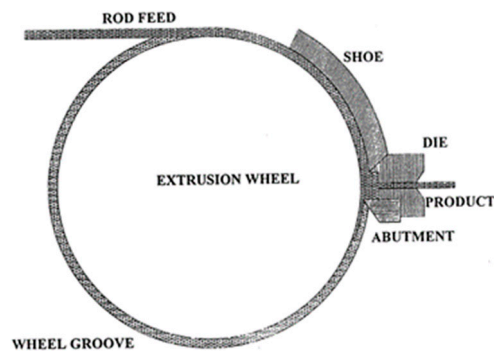


Figure 1. Schematic diagram of the conform.

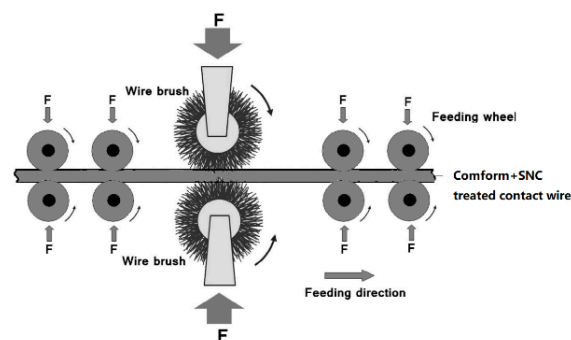


Figure 2. Schematic diagram of surface nanocrystallization.

All SNC samples subjected to corrosion tests were covered by epoxy resins, leaving a columnar exposed area of 9 cm². 0.1 M NaCl aqueous solution was used for corrosion tests. Immersion tests were carried out at room temperature for 30 days in an open system. The corrosion morphologies of the samples were observed via a digital microscope (Hirox, KH-7700, Hackensack, NJ, USA) and the scanning electronic microscope (SEM, S-3400N, Hitachi, Tokyo, Japan). The chemical composition of the corrosion product was characterized by the energy-dispersive X-ray spectrometer (EDS, OXFORD instrument, Oxford, Oxfordshire, UK). After the set intervals of immersion, the mass loss of the samples was examined by an electronic balance (accuracy: 0.1 mg) to calculate the corrosion rate (unit: mg·cm⁻²·h⁻¹) of the SNC-treated alloy. 5 parallel samples were used in this test to get the average corrosion rate of the alloys with and without SNC treatment.

Electrochemical corrosion behavior of SNC samples were evaluated by a CHI660D advanced potentiostat (Huacheng, Shanghai, China) equipped with a saturated calomel electrode (SCE) and a Pt counter electrode. For better repeatability, more than three parallel samples were conducted in each electrochemical test. The samples were freely immersed in the solution for 1000 s to obtain the stable open circuit potential (OCP) values. The frequency of electrochemical impedance spectroscopy (EIS) tests ranged from 10 KHz to 0.01 Hz, and the amplitude of the sinusoidal potential signal was 5 mV with respect to the OCP value of the samples. The potentiodynamic polarization (PDP) tests were performed at a scan rate of 1 mV/s, which started at a potential value 250 mV below the obtained OCP value.

3. Results

3.1. Microstructure Characterization of Cu-0.4%Mg Alloy

Figure 3 presents optical microstructures of the conformed Cu-0.4 wt.%Mg before and after SNC processing. As shown in Figure 3a, the α -Cu grains of the conformed alloy equiaxed and reached

an average size of 8 μm . The alloying Mg element in small quantities was solid solutions, thus no second-phase particles exist in the copper matrix. During the continuous conform procedure, the temperature in the die chamber reached as 800 $^{\circ}\text{C}$ and was significantly higher than the recrystallization temperature (about 350 $^{\circ}\text{C}$) of the Cu-Mg alloy. Therefore, the grain size of the alloy subjected to the conform procedure could not reach nanometers for dynamic recrystallization. As shown in Figure 3b,c, the surface grains after SNC treatment are obviously fine, and there is a gradient microstructure in the longitudinal section of the alloy. The surface area underwent severe plastic deformation during SNC treatment, resulting in the formation of a fibrous, deformed microstructure. More information on the SNC gradient microstructure, especially the nano-grains, can be obtained from TEM observation.

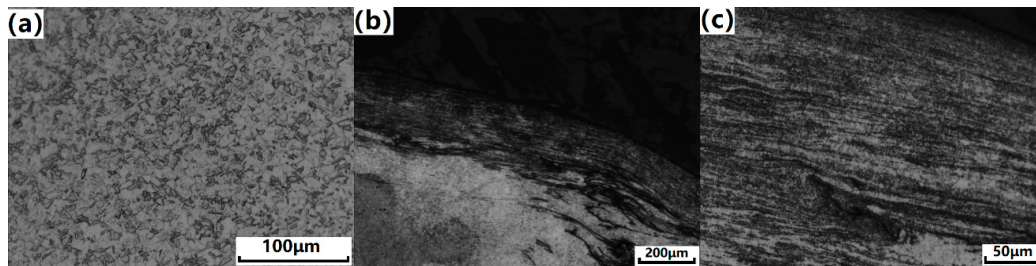


Figure 3. Optical microstructures of the Cu-Mg alloy at (a) the as-conformed state; (b) and (c) are the conform + surface nano-crystallization (SNC) alloy at low and high magnification, respectively.

Figure 4 presents the TEM micrograph of severely deformed α -Cu grains after SNC treatment. It is clear that the α -Cu grains have been further refined into equiaxed nano-grains with an average size of 400 nm. The white areas at the arrowheads in Figure 4a are the low-density zones (LDDZ) of dislocations, which is a typical microstructural characteristic in nanostructured copper samples [18,19]. As is well-known, dislocation tangling is frequently observed in the grain interior of heavily strained alloys. During the SNC procedure, dislocation proliferation which occurred on the alloys' surface generated high-density dislocations, a mass of dislocation cells, and evident dynamic-recrystallization phenomena. Thus, the formation of the LDDZ areas should be attributed to the dynamic equilibrium between the production and annihilation of the dislocations, as well as the dislocation absorption at the grain boundaries with the grain refinement [20,21]. Plenty of approximately equiaxed dislocation cells increasingly formed subgrains during SNC, and eventually, the subgrain boundaries became low-angle grain boundaries (GBs) and even high-angle GBs. In essence, the severely deformed surface reached the nano-scale level after SNC modification. The arrowhead in Figure 4b indicates the deformation twin in particular grains, which is created by the shear stress and severe strain during the SNC process. The stress causes the appearance of partial dislocations at the grain boundary, which react to form the parallel twins.

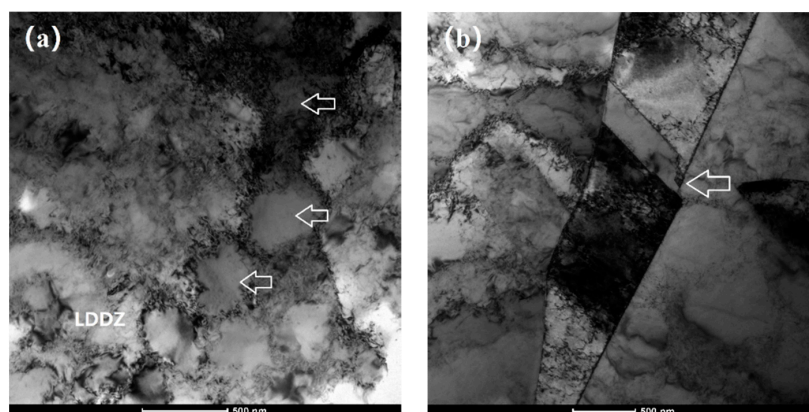


Figure 4. Transmission electron microscopy (TEM) images of the Cu-Mg alloy after SNC: (a) at lower magnification of the dislocation tangle; (b) at higher magnification of the twin zone.

3.2. Electrochemical Results of Cu-0.4%Mg Alloy

Figure 5a presents the continuous OCP monitoring of the alloy with and without SNC treatment, immersed in 0.1 M NaCl solution for 1000 s. It is clear that the OCP values of both untreated and SNC samples decrease rapidly in the initial 200 s, and then decrease slowly during the rest of the immersion time. The surface of the samples were wet soon after immersing the solution, and an electric double layer was formed at the solid–liquid interface. The lower OCP value of the SNC sample presents the higher corrosion tendency in NaCl solution, compared to the conformed sample without SNC treatment.

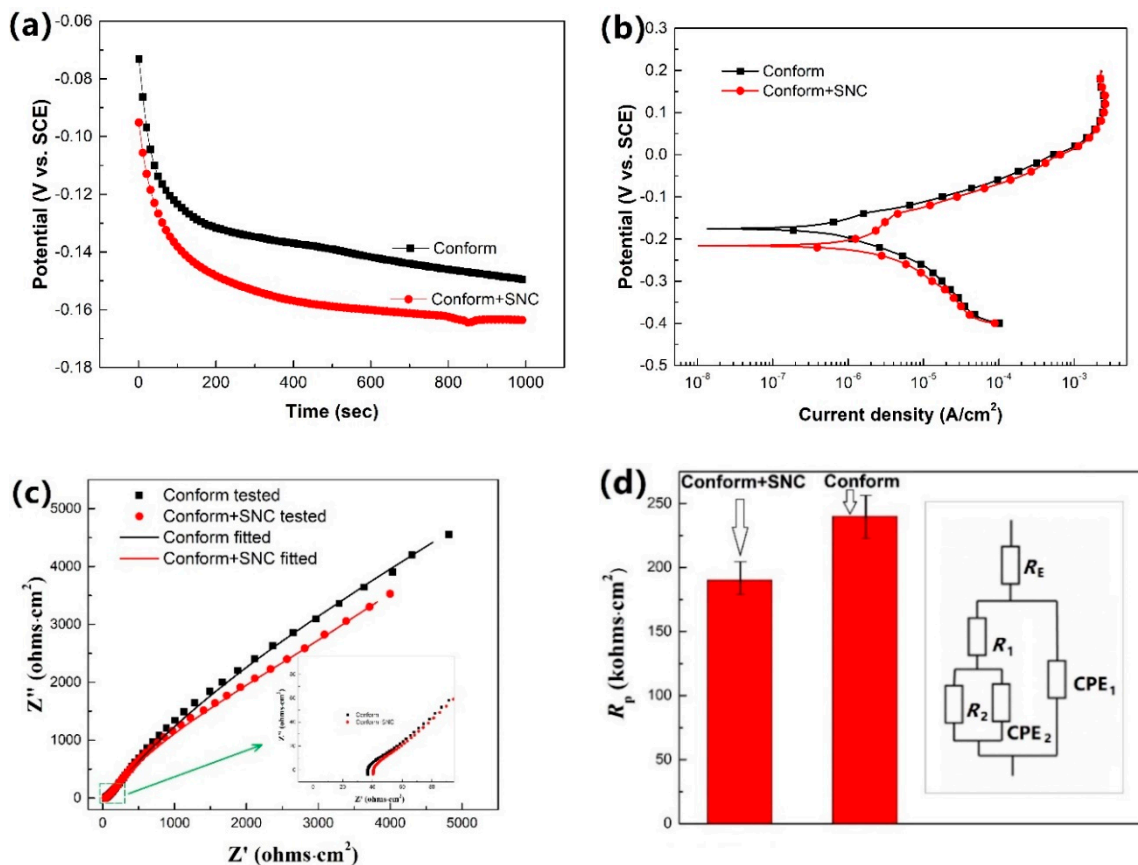


Figure 5. Electrochemical corrosion tests of the conform and conform + SNC Cu-Mg alloy after immersion in 0.1 M NaCl solution for 1000 s. (a) Open circuit potential (OCP) curves; (b) polarization curves; (c) and (d) are the EIS Nyquist plots and the relative equivalent circuit and fitted R_p values.

Figure 5b presents the PDP curves of the untreated and SNC-treated samples immersed in 0.1 M NaCl solution. Before the PDP test, the samples were immersed in the solution for 1 h. Table 1 lists the values of corrosion potential (E_{corr}) and corrosion current density (I_{corr}) determined by the Tafel extrapolation procedure from Figure 5b. The similar characteristics of the PDP curves indicates the same corrosion mechanism of the untreated and SNC-treated Cu-Mg samples, which shows up as anodic activation dissolution in the NaCl solution of low concentration. It is well-known that a nobler corrosion potential leads to lower corrosion tendency in thermodynamics, and a higher corrosion current density elucidates a faster corrosion rate in corrosive medium. As seen in Table 1, the SNC sample has a lower E_{corr} value and higher I_{corr} value, in comparison with the untreated sample. It also indicates that the SNC sample is more readily attacked by NaCl solution in the initial.

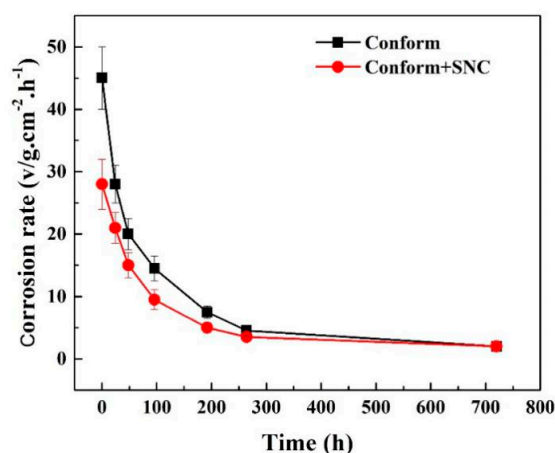
Table 1. Electrochemical parameters of conform and conform + SNC samples immersed in 0.1 M NaCl solution.

Samples	E_{corr} (V _{SCE})	I_{corr} (μA/cm ²)
Conform	-0.176 ± 0.01	0.65 ± 0.05
Conform + SNC	-0.216 ± 0.01	0.15 ± 0.03

Figure 5c presents the typical Nyquist impedance plots of the untreated and SNC-treated samples at open-circuit potential after 1000 s immersion in 0.1 M NaCl solution. The similar Nyquist plots represent that the corrosion mechanism of the alloy has not changed after SNC treatment. The line going upwards with slope one in the low-frequency region indicates a diffusion-controlled process. The high-frequency region of the EIS Nyquist plots is shown in the bottom right corner of Figure 5c. The diameter of the capacitive loop is widely accepted to typify the polarization resistance value of the double layer. The SNC samples presents a lower conductive loop diameter, which indicates lower polarization resistance (R_p) after SNC treatment. The $R(Q(R(QR)))$ equivalent circuit was used to fit the EIS plots and to show the used equivalent circuit and fitted R_p values, presented in Figure 5d. Clearly, the R_p value (about 185 kΩ·cm²) of the SNC sample is smaller than that of the conform sample (about 235 kΩ·cm²), indicating that there was less corrosion resistance in the initial corrosion period.

3.3. Immersion Corrosion Results

A constant immersion test of the samples, followed by a mass-loss measurement and optical microscopy, provided concrete evidence for electrochemical corrosion behavior. Figure 6 presents the mass-loss rate of the untreated and SNC-treated samples after long-term immersion in 0.1 M NaCl. It is clear that the change rule of corrosion rate of the two samples are the same in the solution after a certain time. The mass-loss rate of the samples gradually decreased with the rise in immersion time, and finally returned to a relatively stable value. The higher corrosion rate at the initial stage of immersion is due to anodic activation dissolution without a passivation phenomenon. After immersion for some time, the corrosion product film piled up at the surface conferred a protective effect to reduce the corrosion rate. Figure 7 presents the macro-appearance of corroded regions of the untreated and SNC-treated samples after 2 and 15 days of immersion in 0.1 M NaCl. It indicates that there is no typical pitting corrosion phenomenon, but the uniform corrosion characteristic is presented in the two samples with 2 days of immersion. After 15 days of immersion in 0.1 M NaCl, typical corrosion pits could be located on several sites for the conformed sample, but there was slight corrosion dispersed over an area for the SNC sample.

**Figure 6.** Corrosion rates (with duration) of conform and conform + SNC Cu-Mg alloy immersed in 0.1 M NaCl solutions at different times.

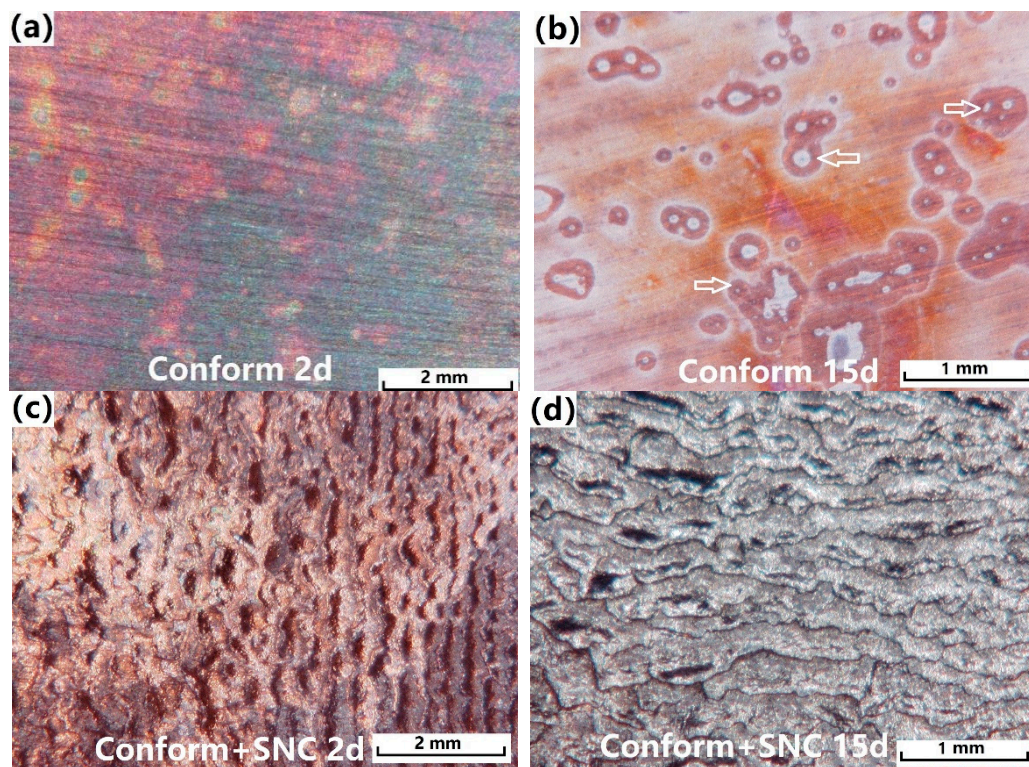


Figure 7. Macro-appearance of the conform and conform + SNC Cu-Mg alloy immersed in 0.1 M NaCl solutions for 2 days and 15 days. (a) Conform sample after corrosion for 2 days; (b) Conform sample after corrosion for 15 days; (c) Conform + SNC sample after corrosion for 2 days; (d) Conform + SNC sample after corrosion for 15 days.

3.4. Influential Mechanism of SNC on the Corrosion Behavior of the Cu-0.4%Mg Alloy

Corrosion behavior and corrosion resistance of the materials were strongly influenced by their surface condition, especially the surface microstructure characteristics and the surface roughness [22,23]. Meanwhile, the environmental factors also had an important impact on the corrosion process. In our former investigation on corrosion behavior of the SNC-treated rebar in a simulated concrete-pore solution, we found that the SNC rebar showed enhanced passivation ability and improved corrosion resistance against Cl^- aggression [16]. Herein, the corrosion behavior of the SNC-treated Cu-Mg alloy seems to be more complicated. It suffered rapid anodic dissolution and showed less corrosion resistance in NaCl solution during the initial corrosion period. However, in long-term corrosion, the SNC-treated alloy showed a decreased corrosion rate and better corrosion resistance compared to the conform alloy. It is possible that the anti-corrosion performance of the SNC-treated alloy was greatly influenced by its SNC microstructure characteristics and surface roughness.

To reveal the effects of grain refinement on the corrosion resistance of the alloy, the XRD analysis was further used to judge the grain size of the alloy before and after SNC modification and corrosion. Before the test, the SNC-modified samples were immersed in 0.1 M NaCl solution for 10 days. From the XRD plots in Figure 8, one can find that all the samples presented with typical copper peaks. Considering the small amount of Mg content, the typical copper peaks can be regarded as the Cu-Mg solid solution. A more detailed difference can be found in the full width at half maxima (FWHM) values of the XRD patterns of the alloys. Many studies have reported that the FWHM values can be used to judge the grain size of the tested materials semi-quantitatively according to the Scherrer equation. Larger FWHM values infers broadening in the diffraction peaks, which denotes a decrease in the surface grain size [24,25]. Herein, the FWHM values of the typical three strongest peaks of the SNC-treated alloy are larger than that of the conform alloy (shown in the Table 2). This phenomenon should be induced by the severe refinement of the surface grains during SNC modification, which will

bring a mass of grain boundaries with high energy. As observed in the TEM images above, dislocation proliferation on the alloys' surface generated high-density dislocations, as well as strain-induced twins, during the SNC process. Since the nature of electrochemical corrosion of copper in NaCl solution leads to active dissolution of the anode, the mass of high-energetic crystal defects (such as grain boundaries, dislocations, and twins) may lead to more residual stress and corrosion activity compared to the conform alloy. These energetic crystal defects provide a more active site for corrosion, leading to more rapid anodic dissolution in the initial corrosion period.

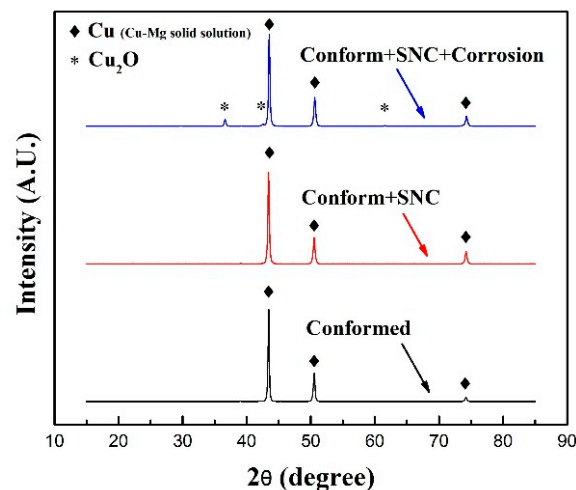


Figure 8. X-ray diffraction (XRD) plots of the conform and conform + SNC Cu-Mg alloys before and after corrosion.

Table 2. Crystallographic parameters of the Cu-0.4%Mg alloys via X-ray diffraction (XRD) analysis.

Peak Angle	FWHM of Conform Alloy	FWHM of Conform + SNC Alloy	FWHM of Conform + SNC + Corrosion alloy
First peak 43.4°	0.248	0.272	0.269
Second peak 50.5°	0.309	0.339	0.338
Third peak 74.2°	0.347	0.389	

As opposed to the conform alloy, there seems to be no change in FWHM values between the SNC samples before and after corrosion. From this phenomenon, one can believe that the corrosion damage of the SNC-treated alloy is quite limited, and the nano-scaled microstructure of this alloy was still kept after corrosion. Besides the copper peaks, the corroded sample also presented with weak Cu_2O peaks. It is generally believed that part of the cathodic process of the electrochemical corrosion of copper is oxygen absorption corrosion, and that the weak Cu_2O peaks should be detected from the corroded products.

It is generally believed that high surface roughness is also harmful to the corrosion resistance of the materials. As shown in Figure 9, the surface roughness of both the conform and conform + SNC samples were quantitatively evaluated by the laser scanning confocal microscope. The typical surface roughness (R_a) of the conform + SNC samples were about 15 μm , nearly 6 times larger than that of the conform sample ($R_a = 2.4 \mu\text{m}$). The more significant surface roughness of the SNC-treated alloy brought a more exposed area to the aggressive medium, leading to more rapid anodic dissolution during the initial corrosion period.

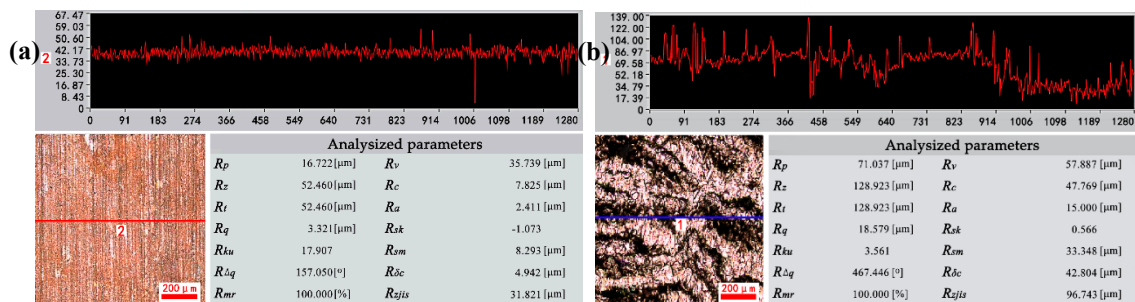


Figure 9. Surface roughness analyzed by the laser scanning confocal microscope. (a) Conform + SNC sample; (b) conform sample.

SEM analysis of the corroded surfaces of alloys after immersion corrosion in 0.1 M NaCl for 30 days was carried out to disclose the anti-corrosion mechanism during long-term corrosion. As shown in Figure 10, the corroded surfaces of the two samples were covered with corrosion products. It is obvious that the surface of the untreated sample was fully covered with more uniform and loose corrosion products, while the surface of the SNC sample was partially covered with more compact corrosion products. The finer grains with higher-density dislocation after SNC treatment provided more active sites for corrosion reaction to form a more compact corrosion production layer. Table 3 shows EDX results obtained from the corroded surface examination of the same samples in Figure 10c,f. For the two samples, the presence of chloride and oxygen was detected, from which one can deduce that CuCl and Cu₂O should be formed. A higher percentage of the O element was obtained on the surface of the Conform+SNC sample, which indicates that, in this case, CuCl formation was somehow inhibited.

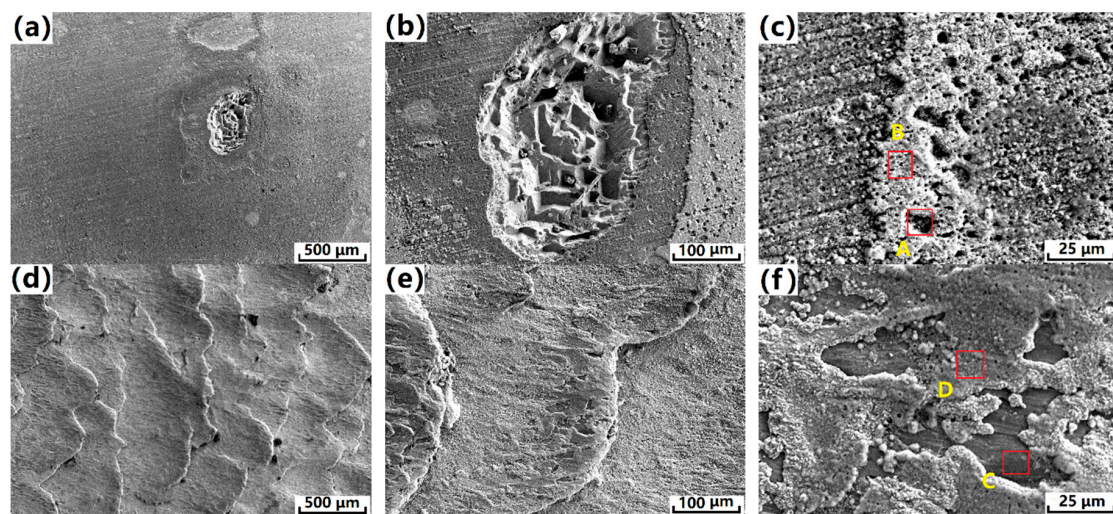


Figure 10. Scanning electron microscopy (SEM) corrosion morphologies of the Conform (a–c) and Conform + SNC (d–f) Cu-Mg alloys' immersion in 0.1 M NaCl solution for 30 days. (a) and (d) are low-magnification images; (b) and (e) are medium-magnification images; (c) and (f) are high-magnification images.

In addition, the conform alloy presented with typical corrosion pits, as shown in Figure 10a,b, which can be related to the corrosion pits observed in the optical corrosion morphologies shown in Figure 7b. It is clear that the corrosion damage in pits has already extended into the deep substrate. Meanwhile, there were no corrosion products covering the pit, which indicates the continuous corrosion damage in the pits during long-term immersion corrosion. Due to the large tensile stress of the contact wire during the service, those corrosion pits on the conform alloy will provide priority nucleation for micro-cracks. Corrosion-induced cracks greatly decrease the fracture toughness of the alloy, which is vital to the safety and lifespan of the contact wire. However, the SNC-treated contact wire has a harder

surface, as well as overall corrosion without pitting corrosion risk; these favorable factors will ensure its superior fracture toughness. Fracture toughness can be carefully extracted by the pillar-splitting method, which enables testing of the fracture toughness for sub-micrometer scale materials or in specific zones for bulk materials [26]. This investigation will be the focus of our future work.

Table 3. Energy dispersive X-ray spectrometer (EDS) analysis of corrosion products on the surface of Conform and Conform + SNC specimens immersed in 0.1 M NaCl solutions for 30 days.

Elements	Atomic Percent %			
	Conform Postion A	Conform Postion B	Conform + SNC Postion C	Conform + SNC Postion D
O	50.14	56.88	54.02	56.40
Cl	24.74	15.42	11.82	14.00
Cu	48.73	27.69	33.98	29.60

4. Conclusions

This work has shown the detrimental effect of surface nanocrystalline modification of Cu-0.4%Mg alloy on their electrochemical corrosion behavior, due to the finer grains and more microstructural defects.

The SNC process, via high-speed rotating wire-brushing, forms the severe deformed plastic flow zones and increased surface roughness. The grain size of the surface deformed zone was refined into a nanometer regime, resulting from the formation of plenty of dislocation cells and deformation twins.

Strains-induced grain refinement weakens corrosion resistance of the SNC alloy during the initial corrosion period in 0.1 M NaCl solution, resulting in the lower OCP value and higher I_{corr} values in polarization tests, a smaller capacitive loop and R_p value in EIS tests, higher mass-loss rate, and a partially corroded surface. The SNC sample with a smaller grain size has lower corrosion resistance, indicating that the increased crystal defects and higher surface roughness results in increased corrosion activity.

However, the SNC alloy presented with a gradually decreasing corrosion rate (mass-loss rate) in the long-term immersion corrosion tests. The improved corrosion-resistance performance of the SNC alloy contributed to the formation of more compact corrosion products on the SNC's surface.

Author Contributions: D.S., J.J. and A.M. conceived and designed the experiments; X.G., Y.Q. and X.L. contributed to the sample preparation and corrosion behavior testing; J.C. and J.S. contributed to the data analysis; D.S. and J.J. wrote the paper.

Funding: This research was funded by the Fundamental Research Funds for the Central Universities (2018B57714 and 2018B48414), Natural Science Foundation of China (51878246), Key Research and Development Project of Jiangsu Province of China (BE2017148), "Six talent Peak" project of Jiangsu Province (2016-XCL-196) and the Public Science & Technology Service Platform Program of Suqian City of China (Grant No. M201614).

Acknowledgments: The study was supported by the Fundamental Research Funds for the Central Universities (2018B57714 and 2018B48414), Natural Science Foundation of China (51878246), Key Research and Development Project of Jiangsu Province of China (BE2017148), "Six talent Peak" project of Jiangsu Province (2016-XCL-196) and the Public Science & Technology Service Platform Program of Suqian City of China (Grant No. M201614).

Conflicts of Interest: The authors declare no conflict of interest.

References

- Peng, L.M.; Mao, X.M.; Xu, K.D.; Ding, W.J. Property and thermal stability of in situ composite Cu-Cr alloy contact cable. *J Mater. Process. Technol.* **2005**, *166*, 193–198. [[CrossRef](#)]
- Zhang, L.; Meng, L.; Liu, J.B. Effects of Cr addition on the microstructural, mechanical and electrical characteristics of Cu-6wt.%Ag microcomposite. *Scr. Mater.* **2005**, *52*, 587–592. [[CrossRef](#)]
- Fernee, H.; Nairn, J.; Atrens, A. Precipitation hardening of Cu-Fe-Cr alloys. *J. Mater. Sci.* **2001**, *36*, 2721–2741. [[CrossRef](#)]
- Liu, J.B.; Zhang, L.; Dong, A.P.; Wang, L.T.; Zeng, Y.W.; Meng, L. Effects of Cr and Zr additions on the microstructure and properties of Cu-6wt.% Ag alloys. *Mater. Sci. Eng. A* **2012**, *532*, 331–338. [[CrossRef](#)]

5. Suzuki, S.; Shibutani, N.; Mimura, K.; Isshiki, M.; Waseda, Y. Improvement in strength and electrical conductivity of Cu-Ni-Si alloys by aging and cold rolling. *J. Alloys Compd.* **2006**, *417*, 116–120. [[CrossRef](#)]
6. Gao, H.; Wang, J.; Shu, D.; Sun, B. Microstructure and properties of Cu-11Fe-6Ag in situ composite after thermo-mechanical treatments. *J. Alloys Compd.* **2007**, *438*, 268–273. [[CrossRef](#)]
7. Zhu, C.C.; Ma, A.B.; Jiang, J.J.; Li, X.B.; Song, D.; Yang, D.H.; Yuan, Y.; Chen, J.Q. Effect of ECAP combined cold working on mechanical properties and electrical conductivity of Conform-produced Cu-Mg alloys. *J. Alloys Compd.* **2014**, *582*, 135–140. [[CrossRef](#)]
8. Duan, Y.L.; Xu, G.F.; Tang, L.; Li, Z.; Yang, G. Microstructure and properties of the novel Cu-0.30Mg-0.05Ce alloy. processed by equal channel angular pressing. *Mater. Sci. Eng. A* **2015**, *648*, 252–259. [[CrossRef](#)]
9. Valiev, R.Z.; Islamgaliev, R.K.; Alexandrov, I.V. Bulk nanostructured materials from severe plastic deformation. *Prog. Mater. Sci.* **2000**, *45*, 103–189. [[CrossRef](#)]
10. Sehiotz, J.; Franceseo, D.D.T.; Jacobsen, K.W. Softening of nanocrystalline metals at very small grain sizes. *Nature* **1998**, *391*, 561. [[CrossRef](#)]
11. McFadden, S.X.; Mishra, R.S.; Valiev, R.Z.; Zhilyaev, A.P.; Mukherjee, A.K. Low-temperature superplasticity in nanostructured nickel and metal alloys. *Nature* **1999**, *398*, 684–686. [[CrossRef](#)]
12. Lu, K.; Lu, J. Nanostructured surface layer on metallic materials induced by surface mechanical attrition treatment. *Mater. Sci. Eng. A* **2004**, *38*, 375–377. [[CrossRef](#)]
13. Balusamy, T.; Kumar, S.; Sankara Narayanan, T.S.N. Effect of surface nanocrystallization on the corrosion behaviour of AISI 409 stainless steel. *Corros. Sci.* **2010**, *52*, 3826–3834. [[CrossRef](#)]
14. Li, Y.; Wang, F.; Liu, G. Grain Size Effect on the Electrochemical Corrosion Behavior of Surface Nanocrystallized Low-Carbon Steel. *Corrosion* **2004**, *60*, 891–896. [[CrossRef](#)]
15. Li, N.N.; Shi, S.Q.; Luo, J.L.; Lu, J.; Wang, N. Effects of surface nanocrystallization on the corrosion behaviors of 316L and alloy 690. *Surf. Coat. Technol.* **2017**, *309*, 227–231. [[CrossRef](#)]
16. Song, D.; Ma, A.B.; Sun, W.; Jiang, J.H.; Jiang, J.Y.; Yang, D.H.; Guo, G.H. Improved corrosion resistance in simulated concrete pore solution of surface nanocrystallized rebar fabricated by wire-brushing. *Corros. Sci.* **2014**, *82*, 437–441. [[CrossRef](#)]
17. Kim, Y.H.; Cho, J.R.; Jeong, H.S. A study on optimal design for CONFORM process. *J. Mater. Process. Technol.* **1998**, *80*, 671–675. [[CrossRef](#)]
18. Gong, N.; Wu, H.B.; Yu, Z.C.; Niu, G.; Zhang, D. Studying Mechanical Properties and Micro Deformation of Ultrafine-Grained Structures in Austenitic Stainless Steel. *Metals* **2017**, *7*, 188. [[CrossRef](#)]
19. Huang, J.Y.; Zhu, Y.T.; Jiang, H.; Lowe, T.C. Microstructures and dislocation configurations in nanostructured Cu processed by repetitive corrugation and straightening. *Acta Mater.* **2001**, *49*, 1497–1505. [[CrossRef](#)]
20. Carlton, C.E.; Ferreira, P.J. What is behind the inverse Hall-Petch effect in nanocrystalline materials. *Acta Mater.* **2007**, *55*, 3749–3756. [[CrossRef](#)]
21. Dalla, T.F.; Lapovok, R.; Sandlin, J.; Thomason, P.F.; Davies, C.H.J.; Pereloma, E.V. Microstructures and properties of copper processed by equal channel angular extrusion for 1–16 passes. *Acta Mater.* **2004**, *52*, 4819–4832. [[CrossRef](#)]
22. Samaniego, A.; Llorente, I.; Feliu, S., Jr. Combined effect of composition and surface condition on corrosion behaviour of magnesium alloys AZ31 and AZ61. *Corros. Sci.* **2013**, *68*, 66–71. [[CrossRef](#)]
23. Lee, S.M.; Lee, W.G.; Kim, Y.H.; Jang, H. Surface roughness and the corrosion resistance of 21Cr ferritic stainless steel. *Corros. Sci.* **2012**, *63*, 404–409. [[CrossRef](#)]
24. Lin, Y.; Pan, J.; Zhou, H.F.; Gao, H.J.; Li, Y. Mechanical properties and optimal grain size distribution profile of gradient grained nickel. *Acta Mater.* **2018**, *153*, 279–289. [[CrossRef](#)]
25. Rai, P.K.; Shekhar, S.; Mondal, K. Development of gradient microstructure in mild steel and grain size dependence of its electrochemical response. *Corro. Sci.* **2018**, *138*, 85–95. [[CrossRef](#)]
26. Ghidelli, M.; Sebastiani, M.; Johanns, K.E.; Pharr, G.M. Effects of indenter angle on micro-scale fracture toughness measurement by pillar splitting. *J. Am. Ceram. Soc.* **2017**, *100*, 5731–5738. [[CrossRef](#)]

